# A Numerical Study of the Interactions between Two Tropical Cyclones

SIMON WEI-JEN CHANG

*Science Applications, Inc., McLean, VA 22102*

(Manuscript received 5 February 1983, in final form 10 June 1983)

ABSTRACT

The interactions between atmospheric vortex pairs are simulated and studied with a nondivergent barotropic model and a three-dimensional tropical cyclone model.

Numerical experiments with nondivergent barotropic vortex pairs show that the relative movements of the vortices are sensitive to the separation distance and the characteristics of the swirling wind of the vortex. No mutual attraction is found in any of the nondivergent, barotropic vortex pairs tested.

Results from the three-dimensional tropical cyclone model show that on a constant $f$-plane with no mean wind, the movements of the two interacting tropical cyclones consist of a mutual cyclonic rotation, attraction and eventual merging, in agreement with Fujiwhara's description. The displacement of one interacting storm in the mutual rotation is proportional to the combined strength of the binary system, but inversely proportional to the size of the storm and to the square of the separation distance. The rate of merging is related to the development of a mean secondary circulation on the radial–vertical plane, and is quite independent of the strength of the two tropical cyclones.

The latitudinal variation of the Coriolis parameter adds a northwest beta drift to the trajectories. Depending on their relative strength and location, the beta drift either speeds up the merging process or separates the two interacting tropical cyclones.

## 1. Introduction

When two tropical cyclones are present simultaneously in the same region, it is often observed that they rotate around each other with decreasing separation between them in the absence of large-scale wind flow (Fig. 1). The phenomenon was made well-known by Fujiwhara (1921), and is therefore referred to as the Fujiwhara effect. By laboratory experiment and geophysical observation, Fujiwhara (1923, 1931) demonstrated that the relative motion of two counterclockwise vortices was a counterclockwise rotation. Haurwitz (1951) examined several tropical cyclone pairs by introducing the concept of center of mass around which the two tropical cyclones rotate about each other. By approximating the circulation around a tropical cyclone with that of a Rankine vortex, Haurwitz (1951) derived a relationship between the rotation rate and the sum of the total mass circulation of the two tropical cyclones. Many discrepancies were found when he applied the relationship to observations. Haurwitz attributed the discrepancies to the influence of large-scale flow and lack of data, which led to analysis deficiencies.

Hoover (1961) studied binary tropical cyclones in both the Atlantic and western Pacific Oceans. He found that the interaction between tropical cyclone pairs in the western Pacific Ocean agrees with Fujiwhara's description while those pairs in the Atlantic Ocean rotated in an anticyclonic sense. He suggested that the different large-scale atmospheric flow patterns in the two basins may have caused the binary systems to behave differently. The influence of the large-scale flow was also noted by Liu and Wang (1966). They found that two interacting tropical cyclones in the western Pacific are not always attracted to each other when there are strong shears in the environmental flow. Recently, Dong and Neumann (1983) found that storm pairs exhibiting behavior most in accordance with Fujiwhara's description were located in the Intertropical Convergence Zone (ITCZ) where horizontal shears in large-scale flow are negligible. They suggest that the effects of environmental flows be filtered before the real Fujiwhara effects can be determined. But to define and remove the large-scale flows from observational data is difficult to accomplish.

Over the 35-year period 1946–81, storm pairs known to have interactions averaged 1.5 annually in the western North Pacific and 0.33 annually in the Atlantic (Dong and Neumann, 1983). The presence of binary interaction has been noted to have contributed to forecast errors of tropical cyclone tracks (Brand, 1970; Jarrell *et al.*, 1978; Neumann, 1981). Forecasting as well as analyzing a single tropical cyclone is often hindered by the paucity of observational data in the tropical cyclone basin (Neumann, 1981); the presence of two storms in close proximity can further compound the difficulties.

The purpose of our study is to investigate the interactions between two tropical cyclones by numer-

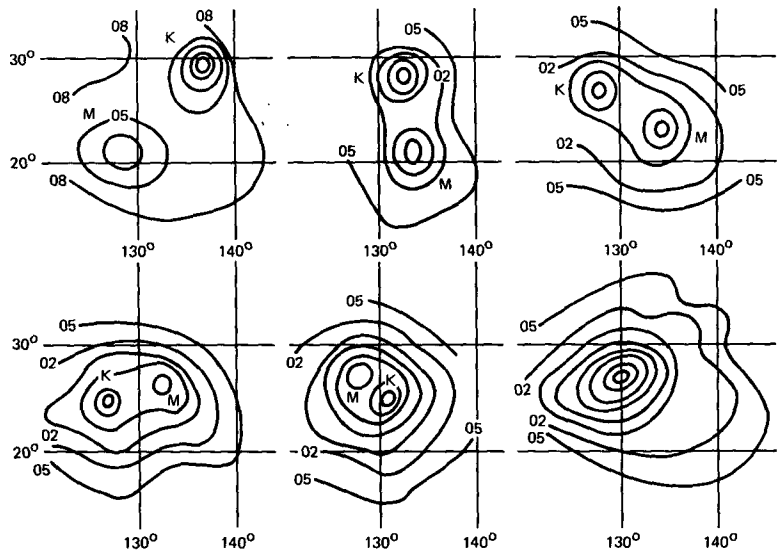


FIG. 1. Surface isobaric analyses at 0000 GMT 15–20 September 1964 showing the rotation and merging of typhoons Kathy (K) and Marie (M). Isobars are plotted every 3 mb. (From Liu and Wang, 1966).

ical simulations. Because the spatial resolutions of the models are better than the current observational network, and because numerical models can be controlled to produce "clean" results void of undesirable factors, analyzing realistic numerical simulations can sometimes result in a better isolation and understanding of the phenomenon than can be achieved from an observational approach. In this paper we will first determine the role of vorticity advection between the two vortices. For this purpose, a nondivergent, barotropic model is introduced to test two types of vortex pairs with different swirling winds. These barotropic tests will be presented in Section 2. In Section 3, three-dimensional simulations of the interactions between two diabatically driven tropical cyclones on a constant $f$-plane and with variable $f$ will be discussed. Our findings will be summarized in Section 4.

## 2. Interactions between nondivergent, barotropic vortex pairs

In this section, we investigate the interactions between nondivergent barotropic vortex pairs. Through the interactions of such vortex pairs, we can determine the contribution of horizontal advection of vorticity, because in such a system advection is the only mechanism for interaction. A description of the nondivergent, barotropic model will be presented first, and the experimental design and the results will then be discussed.

### *a. Nondivergent barotropic model*

The simple nondivergent, barotropic model can be described as

$$\frac{\partial}{\partial t}\nabla^2\psi = -\mathbf{V}_\psi \cdot (\nabla\psi + f), \tag{1}$$

$$\mathbf{V}_\psi = \hat{\mathbf{k}} \times \nabla\psi, \tag{2}$$

where $f$ is the Coriolis parameter, $\psi$ the streamfunction, $\mathbf{V}_\psi$ the nondivergent wind, and $\hat{\mathbf{k}}$ a vertically pointing unit vector. The boundary conditions for (1) and (2) are Neumann, i.e., $\nabla^2\psi = 0$ at boundaries. The model has $51 \times 51$ grid points with a uniform horizontal resolution of 50 km. The relevant elliptic equation

$$\nabla^2\psi = \zeta, \tag{3}$$

where the relative vorticity is defined by

$$\zeta = \hat{\mathbf{k}} \cdot \nabla \times \mathbf{V}_\psi, \tag{4}$$

is solved by a stabilized error vector propagation method (Madala, 1978).

### *b. Experimental design*

The major application of the nondivergent barotropic model is to determine the effects of separation distance and the radial distribution of tangential winds on the interaction of the two vortices. Two kinds of wind distributions were tested. The first kind (type A) of vortex is defined by its cyclonic swirl wind $v_0$ as a function of radius $r$ from the vortex center, i.e.,

$$v_0 = \begin{cases} Ar\left(1 - \sin\dfrac{\pi r}{r_0}\right), & 0 \leq r \leq r_0 \\ 0, & \text{otherwise,} \end{cases} \tag{5}$$

where the constant $A = 4 \times 10^{-4}$ s$^{-1}$ and $r_0 = 400$

km. Eq. (5) yields a maximum swirl of ~26 m $s^{-1}$ at $r$ = 150 km, and a maximum vorticity $\zeta \approx 7.2 \times 10^{-4}$ $s^{-1}$ at $r = 0$. We note that there is a cutoff of $v_0$ at $r_0$.

The second kind of vortex (type B) is defined as

$$v_0 = Br \exp\left(\frac{r^2}{r_e^2}\right), \quad (6)$$

where the $e$-folding distance $r_e$ is 150 km. By letting the constant $B = 3.6 \times 10^{-4}$ $s^{-1}$, Eq. (6) yields a vortex with strength similar to that described by (5) with maximum swirl of ~29 m $s^{-1}$ and a maximum $\zeta \approx 7 \times 10^{-4}$ $s^{-1}$. The type B vortex differs from type A in that there is no cutoff of swirl. Fig. 2 compares the radial distributions of relative vorticities described by (5) and (6).

Four initial separation distances (300, 400, 600 and 1000 km) have been tested for each type of vortex pairs. All integrations with the barotropic model are performed with constant $f = 4.37 \times 10^{-5}$ $s^{-1}$.

### c. *Results*

Fig. 3 shows the trajectories of storm pairs having two types of swirl wind at four separation distances. It is very clear from Fig. 3 that the smaller the separation distance the faster the mutual transport. For instance, at a separation distance of 1000 km, neither type A vortex pair (with swirl cutoff at $r$ = 300 km) nor type B vortex pair can induce mutual motion. But at a separation distance of 400 km, they move at a speed of ~400 km $day^{-1}$.

It is also evident that the mutually-induced motions of type A and B vortices are very different, despite the values of constants for $A$ and $B$ which were chosen to give vortices of similar strength. Furthermore, the trajectories of the type A vortex pairs are more anticyclonic. This may be a result of the fact that type B vortices have positive vorticities at $r \leq 200$ km, whereas the vorticities of type A vortices change sign at $r$ = 150 km (Fig. 2). Only vortex pairs at small separation distances rotate in a cyclonic fashion because they interact with positive shears. The motion of vortices in our model can only be caused by the advection of vorticity, the shear in one vortex generally determines the movement of the other. These results indicate that the mutual motion of an interacting, nondivergent, barotropic vortex pair is quite sensitive to the characteristics of the swirl winds.

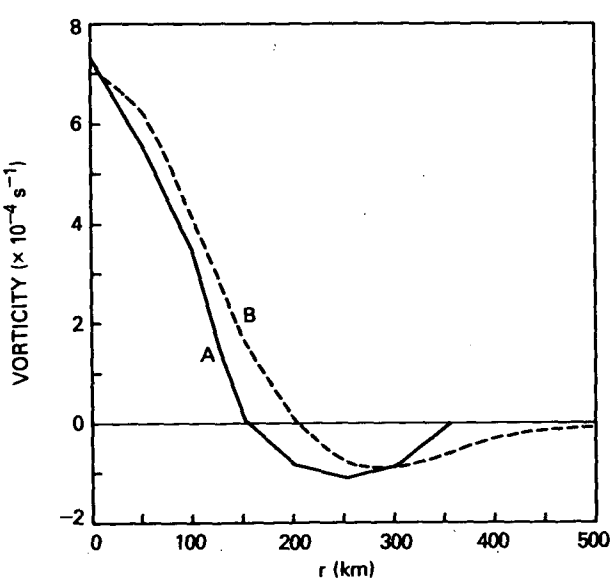


FIG. 2. The radial distribution of relative vorticity for type A (solid) and type B vortex (dashed).

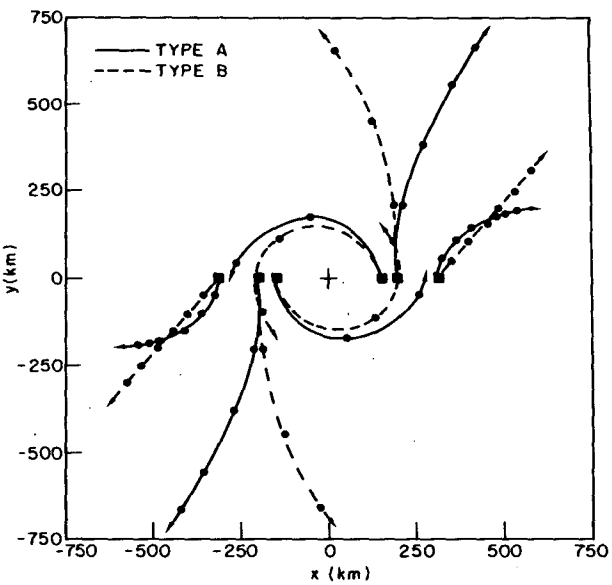


FIG. 3. The trajectories of type A (solid lines) and type B (dashed lines) vortices at separation distances of 300, 400, 600 and 1000 km. The cross is the center of the domain. The time interval between two adjacent dots is 12 h. Squares denote the initial vortex centers.

In all the experiments illustrated in Fig. 3 the storm pairs drift apart, and there is no mutual attraction as observed in some interacting typhoons. This suggests that the observed mutual attraction in typhoon pairs may be due to the divergence and/or convergence that is not included in the barotropic model. Indeed, complicated diabatic processes in tropical cyclone such as longwave radiation, surface boundary layer effects and moist convection generate convergent flow in the lower troposphere and divergent flow in the upper troposphere. The irrotational component of the vortex circulation may be responsible for the occurrence of the observed cyclonic rotation and mutual attraction.

## 3. Interactions between tropical cyclone pairs

We have seen that nondivergent pairs do not cause a mutual motion similar to the description of Fuji-

whara. The observed Fujiwhara effects may be due to dynamics that can only be resolved by a more complete model. To see that, we will simulate the interactions between two diabatically driven tropical cyclones with a three-dimensional model.

### *a. Three-dimensional tropical cyclone model*

The baroclinic model is identical to the one in Chang and Madala (1980) and Chang (1982), except for parameterization of the latent heating. The governing equations are in surface-pressure-weighted flux form for conservation of momentum, temperature and water vapor. The normalized pressure $\sigma = p/p_s$ is the vertical coordinate, where $p_s$ is the surface pressure. The system is assumed hydrostatic. The bulk-boundary-layer parameterization is based on a generalized similarity theory (Chang, 1981). The model has 51 × 51 horizontal grid points with seven sigma layers in the vertical. The horizontal resolution is 0.5° in both latitudinal and longitudinal directions. The east–west boundaries are cyclic. The boundary conditions at the north and south boundaries are such that the second derivatives of thermodynamic variables normal to the boundaries vanish. In addition, diffusion coefficients are increased near the north and south boundaries to damp numerical noise there.

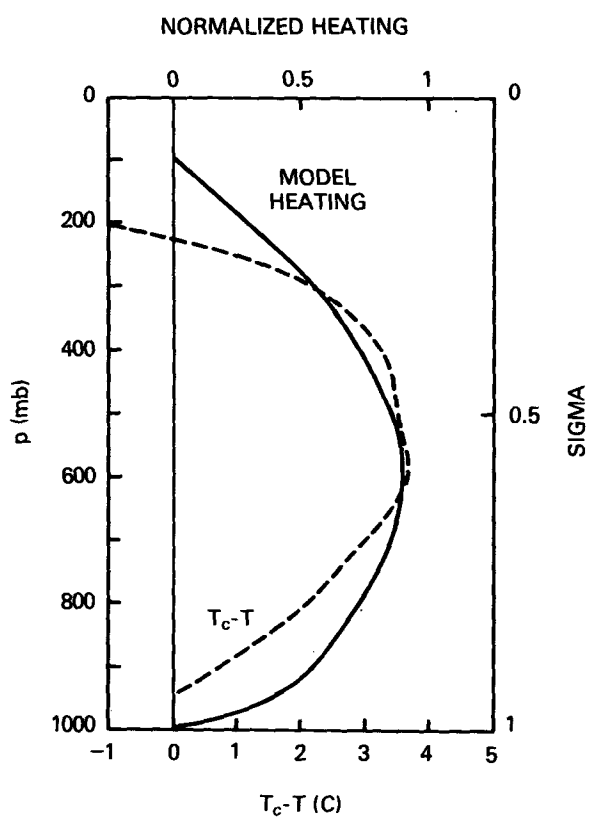


FIG. 4. The vertical distribution of heating used in the model plotted on an arbitrary scale (solid), as compared with ($T_c - T$) for mean hurricane sounding produced by a one-dimensional cloud model (Anthes, 1977, Fig. 4a).

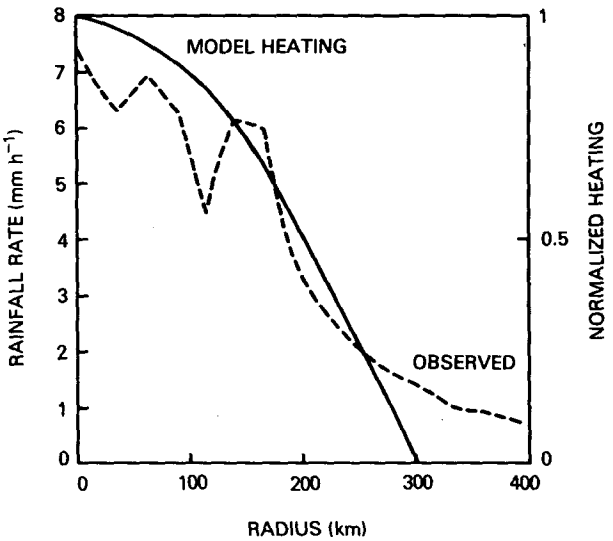


FIG. 5. The horizontal distribution of heating used in the model plotted on an arbitrary scale (solid), as compared with the observed radial distribution of rainfall rate in a typhoon (Adler and Rodgers, 1977, Fig. 5).

Kuo's parameterization was used in Chang and Madala (1980) and Chang (1982), but a prescribed heating is applied in this model as done by Anthes (1971) in an axisymmetric model. The heating rate here is defined as

$$\dot{Q}(r, \sigma) = \begin{cases} \dot{Q}_0 \cos\left(\dfrac{\pi r}{2R}\right) \sin[\pi(\sigma - 0.1)], \\ \quad \text{for} \quad r \leqslant R, 0.1 \leqslant \sigma \leqslant 0.9 \\ 0, \quad \text{otherwise} \end{cases} \tag{7}$$

where $r$ is the distance between a grid point and the low pressure center, and $R$ = 300 km is the limit of the heating function. Two values of $\dot{Q}_0$, 100 and 200 K day$^{-1}$, have been used in various numerical experiments to define the weak and strong tropical cyclones, respectively. The vertical and horizontal distributions of the heating pattern described in (7) are illustrated in Figs. 4 and 5. The vertical heating distribution is similar to that of the differences between temperatures in convective clouds ($T_c$), and the environment ($T$), in a mean hurricane season sounding for the Gulf of Mexico as computed by a one-dimensional cloud model (Anthes, 1977, Fig. 4a). The horizontal heating distribution agrees with the mean rainfall rate inferred from satellite observation in a typhoon (Adler and Rodgers, 1977), except for the observed smooth falloff at $r \geqslant 300$ km. No effort is made to simulate the eye because of the model horizontal resolution.

The heating prescribed by (7) nevertheless generates realistic circulations for tropical cyclones. Fig. 6

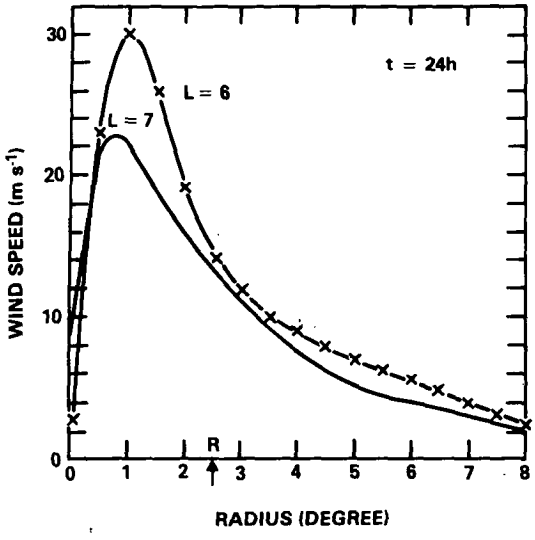


FIG. 6. The radial distribution of the quasi-steady wind speeds in model layer six ($\bar{\sigma}$ = 0.85) and seven ($\bar{\sigma}$ = 0.965) generated by the stationary prescribed heating.

shows the radial distribution of the quasi-steady wind speeds at the sixth ($\bar{\sigma}$ = 0.85) and seventh ($\bar{\sigma}$ = 0.965) model layers after 24 h of heating with $\dot{Q}_0$ = 200 K day$^{-1}$. The wind speeds have a peak at $r$ = 1° and decrease gradually outward without discontinuity at $r = R$ = 300 km.

We note, however, that by using the prescribed heating in (7) the effects of the interaction between the two cyclones on the scale of cumulus convection cannot be adequately simulated. In reality the momentum field in each storm, which affects the cumulus convection, can be modified by the proximity of another storm. A change in the cumulus convection in each storm may alter the storm's intensities, which can in turn affect the interaction between the two tropical cyclones. But these feedbacks may be secondary and are only important when the separation of the two storms is small. As a preliminary study, the more economical, prescribed heating is used to investigate the first-order effects in the interaction.

### b. Experimental design

The tropical cyclone pairs in all numerical experiments (Table 1) with the three-dimensional model are dynamically initialized by a 24 h stationary heating at two locations, i.e., by applying (7) at two fixed grid points for 24 h. Dong and Neumann (1983) found that in real cases when the separation distances are less than 11° latitude, cyclonic rotation predominates. Therefore, the two fixed grid points for the stationary heating are set 10° longitude apart in all experiments to ensure the occurrence of interaction. After the dynamic initialization period, the heating patterns are allowed to follow the low pressure centers. In Experiments 1–3 we simulate the Fujiwhara effects in zero large-scale winds on a constant $f$-plane for strong–strong (Exp. 1), weak–weak (Exp. 2) and strong–weak (Exp. 3) storm pairs. Exps. 1 and 3 are repeated in Exps. 5 and 6 on a real variation of $f$. There is only one single tropical cyclone in Exp. 4 to help isolate the effect of the beta-drift. Unlike on a constant $f$-plane where geophysical orientation is not meaningful, the interactions with real $f$ for a weak (west)–strong (east) pair, and strong (west)–weak (east) pair are quite different, as we shall see later; thus Exp. 7 is conducted to study the latter situation.

### c. Results on a constant f-plane

Fig. 7 shows the surface pressure field at 24, 48, 72 and 96 h for Exp. 1. The southward displacement of storm A (west) and the northward displacement of storm B (east) at 24 h indicate that their interaction has already caused the two storms to begin to rotate cyclonically in spite of the stationary heating. The merging of the two storms progresses with the merging of the outer isobars as observed (Fig. 1). By 96 h, only the 996 mb isobars show two separate low pressure centers. The pressure at the center point of the model decreases by 10 mb while the approaching of the two initial low pressure centers between 24–96 h can only account for a pressure decrease of 2 mb. This indicates that the mutual rotation and merging involve dynamics more complicated than merely advective processes.

TABLE 1. List of three-dimensional numerical experiments.

| Experiment | $\dot{Q}$ (K day$^{-1}$) Storm A | $\dot{Q}$ (K day$^{-1}$) Storm B | $f$ ($s^{-1}$) | Characteristic |
|---|---|---|---|---|
| 1 | 200 | 200 | $4.37 \times 10^{-5}$ | strong–strong interaction |
| 2 | 100 | 100 | $4.37 \times 10^{-5}$ | weak–weak interaction |
| 3 | 100 | 200 | $4.37 \times 10^{-5}$ | weak–strong interaction |
| 4 | 200 | — | variable $f$ | beta drift |
| 5 | 200 | 200 | variable $f$ | strong–strong interaction |
| 6 | 100 | 200 | variable $f$ | weak–strong interaction |
| 7 | 200 | 100 | variable $f$ | strong–weak interaction |

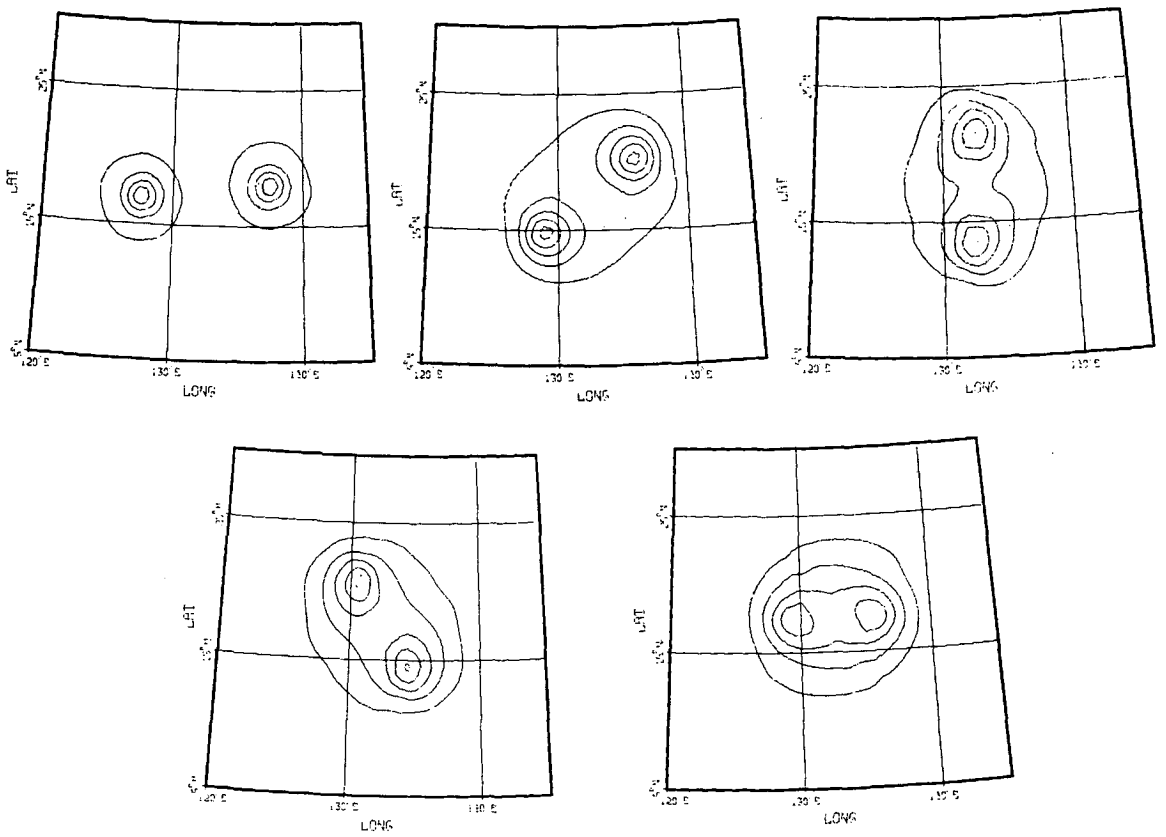


FIG. 7. The surface pressure field at 24, 48, 72, 84 and 96 h. Contour intervals are 4 mb, the outmost closed isobars are 1008 mb. Longitudes are arbitrarily set.

Exps. 1–3 are integrated with a constant $f$. Therefore the orientation has little meaning and the results are independent of the absolute initial positions of the storms. Fig. 8 shows the trajectories of the storm centers in Exp. 1, in which two strong model tropical cyclones are of the same strength. The trajectories show that the two storms rotate about each other in a cyclonic fashion before the coalescence at 102 h. The two trajectories are symmetric about the center of mass, which coincides with the center of the model domain. Superimposed on the symmetric rotation is a convergence of the two tropical cyclones. The distance between the two storms decreases from ~1024 km at 24 h to ~612 km at 96 h. The symmetry remains until 102 h when the two heating patterns overlap and one single large area of low pressure is formed.

Exp. 2 is identical to Exp. 1 except that the heating rate is reduced by one-half. The cyclonic trajectories (Fig. 9) are still remarkably symmetric about the center of mass. Because of the weaker heating, two identifiable centers still exist at 120 h when they are only ~100 km apart. We note again that at small separation distances feedbacks between cumulus convection and the storm pair's interaction have been masked by the prescribed heating in our model.

The speeds at which the two tropical cyclones in Exps. 1 and 2 rotate around and approach each other are shown in Fig. 10. The tangential velocity of the cyclonic rotation in Exp. 1 increases from ~3 m $s^{-1}$

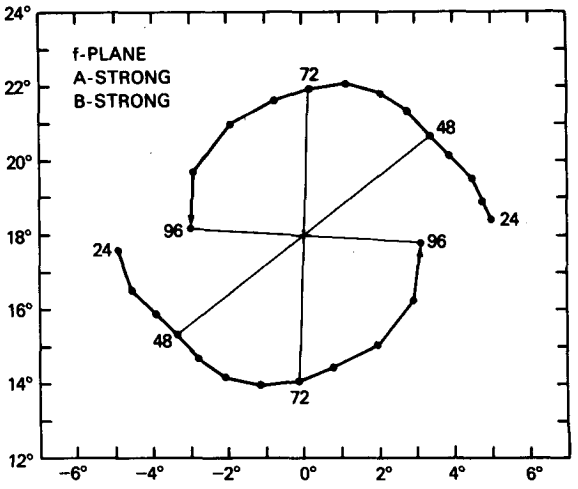


FIG. 8. The trajectories of storm centers in Exp. 1. Numbers on the curve denote times in hours.

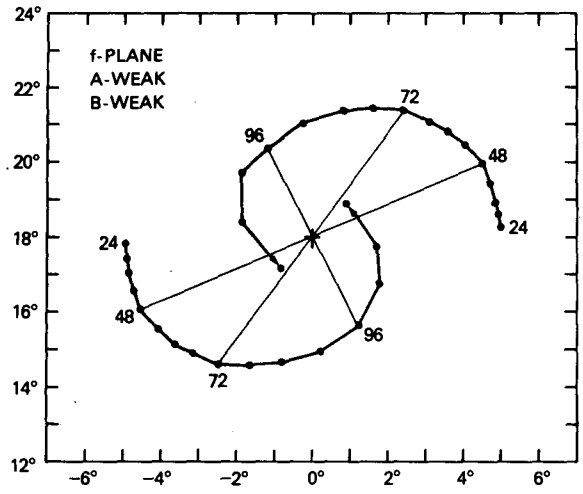


FIG. 9. As in Fig. 8 except for Exp. 2.

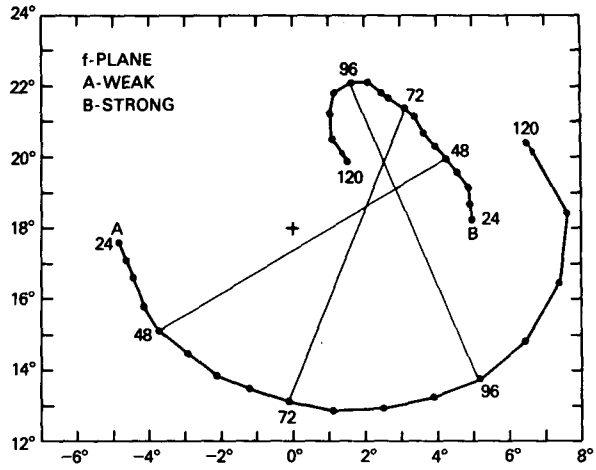


FIG. 11. As in Fig. 8 except for Exp. 3.

at 24–36 h to well over 6 m $s^{-1}$ after 72 h as the separation between the two tropical cyclones becomes small. The rotation speeds in Exp. 2 are ~1 m $s^{-1}$ slower than those in Exp. 1. However, the rate of convergence seems quite independent of the combined strength as indicated by the radial velocities in Fig. 10. The faster rotations between stronger pairs are evident observationally at small separation distances (Dong and Neumann, 1983). At larger separation distances, this relationship is not clear because the observational data contains environmental influences.

Fig. 11 shows the trajectories of the two storm centers in Exp. 3, in which the maximum heating rate in storm A is only half that of storm B. We see that the two storms still rotate about each other cyclonically and that they still move toward each other. However, the trajectories are asymmetric and the weaker storm A moves much faster than the stronger storm B in a way similar to that of a binary celestial system in which the two bodies have different masses. The "mass" of a vortex is perhaps best expressed as the product of its mean angular velocity and the square of an effective radius $\bar{\omega}R^2$. We will discuss this definition later. This type of interaction between storms of different intensities has been observed between Typhoons Flossie and Grace in 1950 (Liu and Wang, 1966). Instead of being stationary, the center of rotation moved within a small area defined by the lines connecting the two storm centers at different times as in Fig. 10.

Results in Exps. 1–3 demonstrate that on an $f$-plane with no large-scale wind, interactions between two tropical cyclones cause the two storms to rotate cyclonically, to attract each other and to coalesce eventually.

In order to examine the momentum fields associated with the interaction we transform the model 500 mb wind fields in Exp. 1 onto a polar grid with respect to the center of the model domain. We now define the azimuthal mean velocity as

$$\bar{\mathbf{V}} = (\bar{v}_r, \bar{v}_\theta, \bar{v}_z) = \frac{1}{2\pi}\int_0^{2\pi} (v_r, v_\theta, v_z)d\theta, \qquad (8)$$

where $v_r$, $v_\theta$, $v_z$ are radial, tangential and vertical velocities on the polar grid, and $\theta$ is the azimuthal angle. Fig. 12 shows the mean vertical (upper), tangential (middle) and radial (lower) velocities for Exp. 1 at 24, 48, 72 and 96 h. It is interesting that the mean momentum fields relative to the center of domain shown here are similar to those in weak but intensifying tropical disturbances (Hawkins and Rubsam, 1968). For example, at 24 h there is a maximum mean tangential velocity of ~4 m $s^{-1}$ at $r \approx 600$ km, and a minimum of ~ −2 m $s^{-1}$ at $r \approx 400$ km, reflecting the cyclonic wind fields about the two storm centers. The maximum tangential velocity gradually increases to ~16 m $s^{-1}$ and moves toward the center to a radius ~ 350 km at 96 h. The maximum inflow also develops from 2 m $s^{-1}$ at $r \approx 600$ km at 24 h to ~4 m $s^{-1}$ at $r$

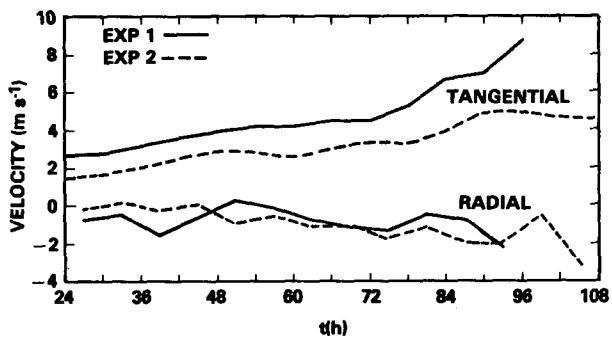


FIG. 10. The tangential and radial speeds of the two interacting tropical cyclones relative to their centers of mass in Exps. 1 and 2.

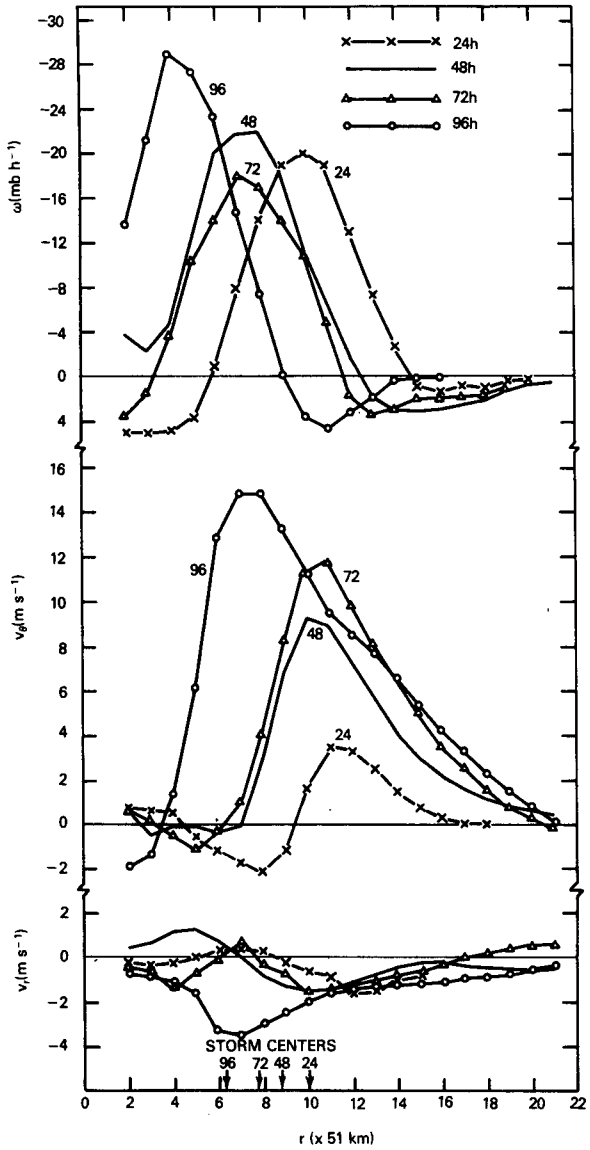


FIG. 12. The azimuthal mean radial ($v_r$), tangential ($v_\theta$) and vertical velocity ($w$) of the wind fields relative to the center of mass in Exp. 1 at 24, 48, 72 and 96 h.

$\approx$ 350 km at 96 h. The evolution of the mean vertical velocity includes the increasing magnitude and contracting radii of maximum upward motion. The development of the mean circulation is accompanied by pressure decrease of 10 mb at the domain midpoint from 24–96 h, as discussed before.

The development of the azimuthal mean circulation can also be illustrated by comparing the kinetic energy (KE) of the mean velocity (KEM) and the KE of the eddy velocity (KEE), where

$$\text{KEM} = \int\int_0^{1000\text{ km}} \tfrac{1}{2}(\bar{v}_r, \bar{v}_\theta)\cdot(\bar{v}_r, \bar{v}_\theta) r dr d\theta, \quad (9)$$

$$\text{KEE} = \int\int_0^{1000\text{ km}} \tfrac{1}{2}(v'_r, v'_\theta)\cdot(v'_r, v'_\theta) r dr d\theta, \quad (10)$$

$$(v'_r, v'_\theta) = (v_r, v_\theta) - (\bar{v}_r, \bar{v}_\theta). \quad (11)$$

As shown by Fig. 13, the KEE, which can mostly be attributed to the circulations around the two centers, reaches a quasi-steady state after 36 h. Meanwhile the KEM, representing the strength of the mean circulation as depicted in Fig. 10 around the center of rotation, steadily increases until the coalescence of the two tropical cyclones. The ratio KEE/KEM decreases from ~3 at 24 h to less than 1 at 96 h.

These analyses suggest that a mean circulation relative to the center of rotation develops due to the interaction of two tropical cyclones. This mean circulation includes tangential, radial and vertical components resembling those associated with tropical cyclones. It is therefore not surprising that the trajectories of the two interacting storms are similar to the trajectories in the hurricane boundary layer (e.g., Anthes 1982, Fig. 4.6). Compared with the nondivergent, barotropic experiments in Section 2, it seems that the diabatic heating in two storms plays a crucial role for the merging of the two storms.

In additional numerical experiments, the surface friction was suppressed to test the frictional effects in the interaction. Results from these experiments were nearly identical to those presented for Exps. 1–3. We also halved the coefficients for the internal dissipation. For the same given heating rates, the interactions are nearly the same except for faster rotation rates, which occur because the model cyclones were stronger with less internal friction. Therefore, neither surface nor internal friction seem to be critical processes in the interactions.

### *d. Relation of mutual rotation rate to bulk parameters of the system*

The results presented so far indicate generally that the rate of the mutual cyclonic rotation depends on

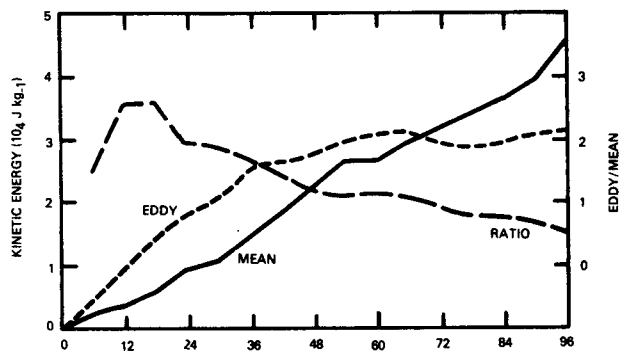


FIG. 13. The development of the kinetic energy of the "mean" flow (solid) relative to the center of mass and the kinetic energy of the "eddy" associated with the two storm centers (dashed) in Exp. 1.

the strength of the binary system and the separation distance of the two interacting storms. Perhaps by relating to some external parameters through laws governing solid-body rotation, a simple description of the numerical results is attainable.

We now consider the rotation of binary storms as similar to that of a dumbbell. The equation of motion for rotation states that the torque $\tau$ acting on the binary system is equal to the product of the rotational inertia of the system $I$ and the angular acceleration $\dot{\omega}$ with respect to the axis of rotation, i.e.,

$$\tau = I\dot{\omega}. \tag{12}$$

If we let $R$ be an effective radius of the storm and $H$ the scale height, the mass of one storm can be approximated by $\rho_0\pi R^2H$. Because the radius of the mutual rotation is about $L/2$, the rotational inertia

$$I \propto \rho_0(\bar{R}_A^2 + \bar{R}_B^2)HL^2, \tag{13}$$

where $\rho_0$ is a reference density and subscripts A and B are pertinent for storms A and B, respectively.

The torque is equal to the cross product of a force and radius of rotation. The force involved in the interaction can be approximated by the advection, then it can be scaled by $\rho_0\bar{V}^2/L$, where $\bar{V}$ is the velocity of the mean circulation defined by (8). Because the mean circulation depends on the combined strength of the two interacting cyclones, therefore $\bar{V} \propto \bar{v}_A + \bar{v}_B$, where $\bar{v}_A$ and $\bar{v}_B$ are the mean wind speed within the effective radius $\bar{R}_A$ and $\bar{R}_B$, respectively. Thus, the torque is proportional to

$$\tau \propto LH\rho_0(\bar{R}_A^2 + \bar{R}_B^2)(\bar{v}_A + \bar{v}_B)^2L^{-1}. \tag{14}$$

We note that the torque contains the dimension of the kinetic energy of the two storms, which is ultimately related to the applied heating $\dot{Q}$ in our model. Substituting (13) and (14) into (12) and dropping the overbars yields

$$(v_A + v_B)^2 \propto \dot{\omega}L^2 \approx f\omega L^2. \tag{15}$$

In the above, $f^{-1}$ is selected as the time scale, so that $\dot{\omega} \approx \omega/T \approx f\omega$. For our purposes of examining numerical results of a limited domain model away from the equator where $f$ remain nearly a constant, the selection of $f^{-1}$ as a time scale is justifiable; then

$$\omega \propto \frac{(v_A + v_B)^2}{fL^2}. \tag{16}$$

Relationship (16) states simply that the rate of the mutual rotation is proportional to the combined kinetic energy of the two interacting tropical cyclones and inversely proportional to the square of the separation distance. In addition, the displacement of one storm should be inversely proportional to its size, because the radius of rotation is inversely proportional to the mass $\pi\rho_0R^2H$.

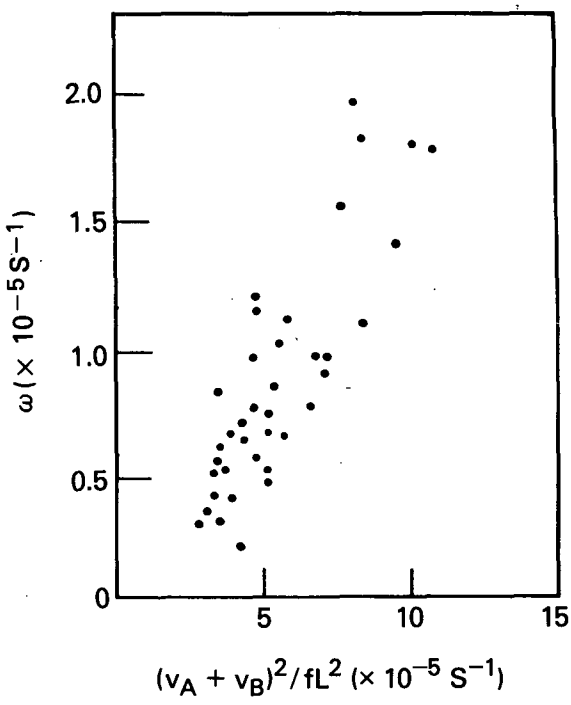


FIG. 14. The rotational rates $\omega$ compared with $(v_A + v_B)^2/fL^2$.

In applying (16) to the numerical results, the mean wind speed within the radius of the gale force wind (17 m s$^{-1}$) is used as $v_A$ and $v_B$. Excluding data when the separation distance is smaller than the sum of two radii of the gale force, rotation rates of binary system at every 6 h were compared with $(v_A + v_B)^2/fL^2$ for Exps. 1–3 (Fig. 14). It is clear the (16) is a good description of the results of Exps. 1–3. The rotation rates $\omega$ and quantities $(v_A + v_B)^2/fL^2$ have a correlation coefficient of 0.81. Therefore, our numerical results can to some extent be represented by the surprisingly simple relationship (16).

It should be noted, however, that (16) is arrived through several simplifying assumptions. These include approximating the mutual rotation of two vortices in the atmosphere by using solid body mechanics and excluding the merging from consideration. While (16) yields good correlation, it is only an approximation of the rotation component of the interaction.

### *e. The effects of variation of the Coriolis parameter*

Exps. 4–7 were carried out with a variable Coriolis parameter, which can produce northwestward drifts of tropical cyclones in the Northern Hemisphere (Adem, 1956; Anthes and Hoke, 1975; Madala and Piacsek, 1975). The velocity of the drift depends on the latitude and the cyclone's circulation. To examine the free drift of a single tropical cyclone in our model, we carried out Exp. 4. As shown by trajectory C in Fig. 15, the model tropical cyclone has an initial

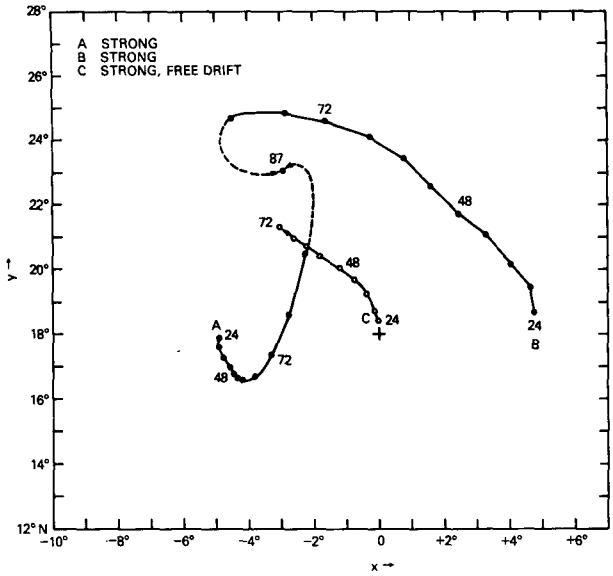


FIG. 15. The trajectories of the free drifting storm in Exp. 4 (curve C) and of the two interacting storms in Exp. 5 (curves A and B).

northward movement, but changes toward the northwest after 36 h, similar to the results of Anthes and Hoke (1975). The 0–72 h mean drift velocity is 1.18 m $s^{-1}$ toward the west and 1.37 m $s^{-1}$ toward the north. The center at 72 h is ~6° to the west, and ~6.5° to the north of the initial position.

The latitudinal variation of the Coriolis parameter has a pronounced effect on the trajectories of the two interacting tropical cyclones. The trajectories of the two tropical cyclones with equal strength in Exp. 5 are shown in Fig. 15. The two storms merge much faster than in Exp. 1, due to the faster northwest drift of the storm located to the south. At 87 h only one large low pressure center is identifiable, while in Exp. 1, two low pressure centers still existed at 96 h (Fig. 7). Instead of rotating around the intersection of the axes as in Fig. 8 for Exp. 1, storm A moves toward the southeast then quickly turns toward the northeast, while storm B rapidly moves northwestward and rotates cyclonically with respect to storm A. The two storms eventually merge into one at 87 h, with storm B having traveled a much longer distance from its initial position than storm A. The relative trajectories of A and B with respect to trajectory C (Exp. 4) are computed. The resultant relative trajectories (not shown) are nearly the same as those in Exp. 1 (Fig. 3), indicating that the trajectories A and B in Fig. 15 are nearly a linear combination of the trajectories in Fig. 3 and the beta drift.

Exp. 6 is to be compared with Exp. 3 where storm A is weaker than storm B. The trajectories of the storm centers in Exp. 6 (Fig. 16) again appear very different from those in Exp. 3. The stronger storm B shows more noticeable northwest drift than in Exp. 3. The weaker storm A rotates cyclonically toward the southeast at a much reduced rate and with a smaller radius, apparently due to the counteracting beta drift.

Most interesting is Exp. 7, in which storm A is stronger than storm B. From 24 to 72 h the weaker storm B moves cyclonically relative to storm A. In the meantime storm A moves slowly toward the southwest nearly perpendicular to and away from storm B. The trajectories take an unexpected turn after 72 h because the two storms now are close to the boundaries and start to influence each other through the east–west boundaries because of the cyclic boundary conditions there.

The distinctively different behavior of Exps. 5–7 can be explained by examining schematically the vectors of forces upon each storm. We let the northwest drift be proportional to the storm's intensity and size (Rossby, 1948; Adem, 1956) and the force due to the interaction be proportional to the combined strength of the binary system but inversely proportional to the strength of the individual storms as discussed in Section 3c. Fig. 17 shows the vectors and the resultant directions of movements for storm A at 24 h of Exps. 5–7. In Exp. 5 both the beta drift and interaction (both the rotation and convergence are accounted for) are strong, the movement of the storm is mostly due south as evident in Fig. 15. In Exp. 6, the beta drift is weaker but the interaction is the strongest, and the movement is nearly along the vector of the interaction. In Exp. 7, the beta effect is strong while the interaction is weak, resulting in a slow movement of the storm away from storm B.

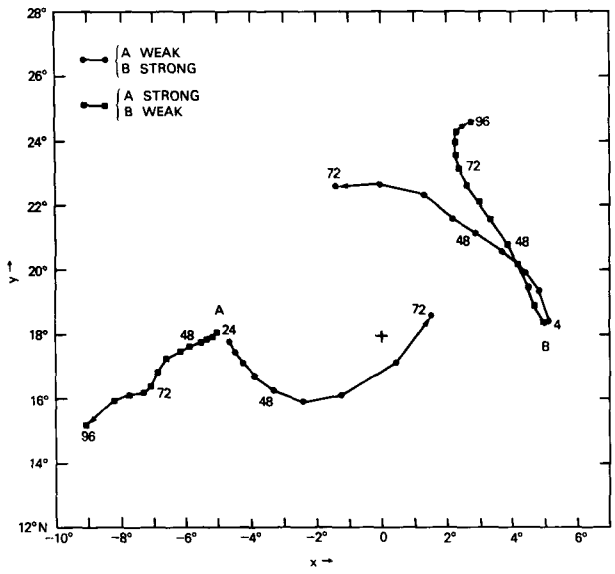


FIG. 16. As in Fig. 15 except for Exps. 6 (solid lines with dots), and 7 (solid lines with squares).

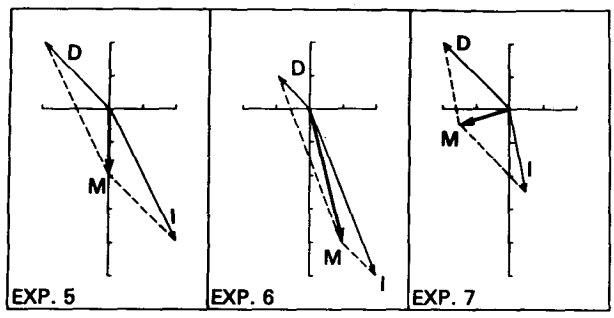


FIG. 17. Vectors showing schematically the force of interaction (*I*), betal drift (*D*), and the resultant movement (*M*) for tropical cyclones A at 24 h of Exps. 5, 6 and 7.

## 4. Summary

The interactions between two mesoscale cyclonic vortices in the absence of large-scale winds have been investigated with a nondivergent, barotropic model and a three-dimensional model. Model results indicate that the interactions between a nondivergent barotropic vortex pair are very different from those observed between a tropical cyclone pair, and that our three-dimensional simulations agree with the observed Fujiwhara phenomenon.

Two types of vortex pairs with various initial separation distances have been tested with the nondivergent, barotropic model. No mutual attraction is found in any of the cases tested. The curvature of the mutually induced rotation depends on the radial profile of swirl winds (or vorticities) of each vortex, and the speed of mutually induced motion is a function of separation—the closer the two vortices, the faster they move. This is quite understandable, because in such a nondivergent barotropic model the two vortices can only interact by advection. These numerical experiments suggest that the observed Fujiwhara phenomenon is caused by a more complex mechanism than just vorticity advection.

Our simulations with a three-dimensional model reproduce observed Fujiwhara effects. The trajectories of simulated strong–strong, weak–weak and weak–strong tropical cyclone pairs on a constant *f*-plane all consist of cyclonic rotations and mutual attractions. The rotation rate between two strong tropical cyclones is generally faster than that between a weak pair. The rate of convergence of a weak pair is not slower than that between a strong pair.

Additional analyses show that as the tropical cyclone pair start to interact, there forms a mean circulation about the center of mass of the two storms as the pressure there decreases more than can be expected by simple advective merging. The development of the mean circulation, consisting of a cyclonic tangential flow and an inward radial flow, resembles the circulation in weak but intensifying tropical disturbances. The kinetic energy of this mean circulation grows by a factor of 4 in 72 h in one experiment, while the kinetic energy of the circulations associated with individual tropical cyclone remains relatively unchanged. It suggests that the development of a mean circulation on the vertical–radial plane relative to the center of mass of the interacting storm pairs is crucial in generating the cyclonic mutual rotation and merging.

A simple analysis points out that the displacement of one tropical cyclone interacting with another is proportional to the combined strength of the vortex pair and inversely proportional to its own size and to the square of the separation distance. Our model results fit this description well except for cases when interacting storms become highly asymmetric about their own centers.

The latitudinal variation of the Coriolis parameter (beta effect) has a large influence on the trajectories of the interacting storm pairs. The beta effect causes a northwest shift and a faster merging of the two tropical cyclones of equal strength. The trajectories of two interacting tropical cyclones of equal strength have a northwest drift superposed on the symmetrical trajectories found on the constant *f*-plane. Observational studies have shown that typhoon pairs sometimes drift away from each other if there were strong shears in large-scale flow (Liu and Wang, 1966; Dong and Neumann, 1983). This study has indicated that differential beta drifts can also cause the two interacting tropical cyclones of different strength to diverge when the one initially located to the west is stronger.

These findings should not be accepted without caution because of several limitations of the numerical model. The model domain is perhaps too small for two tropical cyclones. In addition, the horizontal resolution of 0.5° is only marginal for resolving realistically the smaller scale dynamics near the center. Being a uniform grid model, without decreasing the horizontal resolution, the model domain cannot be expanded due to limited computing resources. The cyclic boundary conditions created problems (as evident in Exp. 7) when two storms may have interacted with each other through the east–west boundaries. Perhaps the most serious limitation of our simulation is the heating prescribed *a priori* in the three-dimensional simulations, which may have masked the interactions between two adjacent tropical cyclones on the scale of cumulus convection. However, the development of the mean circulation about the center of mass of the two tropical cyclones occurs at a very early stage of the interaction when the separation is still large. This suggests that the detailed characteristics of cumulus convection in individual storm may not be important in setting up the cyclic rotation and mutual attraction. The use of the prescribed heating was justifiable except at small separations where the

divergent-convergent pattern in each storm may be modified due to the proximity of another one.

In future research, a parameterized convective heating should be utilized to investigate the above mentioned secondary effect of the cumulus convection. In addition, the parameterized heating may react to large-scale winds in a nonlinear fashion. Therefore, the nonlinear effects of large-scale winds on the interactions of two tropical cyclones also ought to be studied. The question of what is the maximum separation distance for a storm pair to interact is also left for future studies when numerical models of tropical cyclones covering a larger domain are constructed.

*Acknowledgments.* I thank Dr. Rangarao V. Madala for discussions and his help in utilizing his stabilized-error-vector-propagation solver program, and Dr. Darrell F. Strobel for reading and commenting on the manuscript. Dr. Richard A. Anthes critically reviewed an earlier version of the manuscript, Mr. Charles J. Neumann kindly provided me his then unpublished paper (Dong and Neumann, 1983) and a copy of the Fujiwhara (1931) paper. Ms. Shoba Yalamanchili typed the manuscript.

The research was supported by ONR Contracts N00014-81-C-2224 and N00014-82-C-2306.

## REFERENCES

Adem, J., 1956: A series solution for the barotropic vorticity equation and its application in the study of atmospheric vortices. *Tellus,* **8,** 364–372.

Adler, R. F., and E. B. Rodgers, 1977: Satellite-observed latent heat release in a tropical cyclone. *Mon. Wea. Rev.,* **105,** 956–963.

Anthes, R. A., 1971: A numerical model of the slowly varying tropical cyclones in isentropic coordinates. *Mon. Wea. Rev.,* **99,** 617–635.

——, 1977: A cumulus parameterization scheme utilizing a one-dimensional cloud model. *Mon. Wea. Rev.,* **105,** 270–286.

——, 1982: *Tropical Cyclones—Their Evolution, Structure and Effects. Meteor. Monogr.,* No. 41, Amer. Meteor. Soc. [ISBN 9-933876-54-8.]

——, and J. E. Hoke, 1975: The effect of horizontal divergence and the latitudinal variation of the Coriolis parameter on the drift of a model hurricane. *Mon. Wea. Rev.,* **103,** 757–763.

Brand, S., 1970: Interaction of binary tropical cyclones of the western North Pacific Ocean. *J. Appl. Meteor.,* **9,** 433–441.

Chang, S. W., 1981: Test of a planetary boundary layer parameterization based on a generalized similarity theory in tropical cyclone models. *Mon. Wea. Rev.,* **109,** 843–853.

——, 1982: The orographic effects induced by an island mountain range on propagating tropical cyclones. *Mon. Wea. Rev.,* **110,** 1255–1270.

——, and R. V. Madala, 1980: Numerical simulation of the influence of sea surface temperature on translating tropical cyclones. *J. Atmos. Sci.,* **36,** 2617–2630.

Dong, K., and C. J. Neumann, 1983: On the relative motion of binary tropical cyclones. *Mon. Wea. Rev.,* **111,** 945–953.

Fujiwhara, S., 1921: The natural tendency towards symmetry of motion and its application as a principle in meteorology. *Quart. J. Roy. Meteor. Soc.,* **47,** 287–293.

——, 1923: On the growth and decay of vortical systems. *Quart. J. Roy. Meteor. Soc.,* **49,** 75–104.

——, 1931: Short note on the behavior of two vortices. *Proc. Physico-Mathematical Society Japan,* Vol. 13, 3rd ser. 106–110. [Available from the Library of Congress, Washington, DC 20540 or the author S. W. Chang.]

Haurwitz, B., 1951: The motion of binary tropical cyclones. *Arch. Meteor. Geophys. Biolkim.* **A4,** 73–86.

Hawkins, H. F., and D. T. Rubsam, 1968: Hurricane Hilda, 1964: I. Genesis, as revealed by satellite photographs, conventional and aircraft data. *Mon. Wea. Rev.,* **96,** 428–452.

Hoover, E. W., 1961: Relative motion of hurricane pairs. *Mon. Wea. Rev.,* **89,** 251–255.

Jarrall, J. D., S. Brand and D. S. Nicklin, 1978: An analysis of western North Pacific tropical cyclone forecast errors. *Mon. Wea. Rev.,* **106,** 925–937.

Liu, D. L., and S. T. Wang, 1966: Case study of interactions of Pacific Ocean typhoons. *Quart. J. Wea. Forecast. Anal.* (in Chinese). [Available from S. T. Wang, Dept. Atmos. Sci., National Taiwan University, Taipei, Taiwan.]

Madala, R. V., 1978: An efficient direct solver for separable and nonseparable elliptic equations. *Mon. Wea. Rev.,* **106,** 1735–1741.

——, and S. A. Piascek, 1975: Numerical simulation of asymmetric hurricane on a $\beta$-plane with vertical shear. *Tellus,* **27,** 453–468.

Neumann, C. J., 1981: Trends in forecasting the tracks of Atlantic tropical cyclones. *Bull. Amer. Meteor. Soc.,* **62,** 1473–1485.

Rossby, C. G., 1948: On displacements and intensity changes of atmospheric vortices. *J. Mar. Res.,* **7,** 175–187.